VERSITA

Acta Geophysica
vol. 56, no. 4, pp. 1109-1128
DOI: 10.2478/s11600-008-0050-x

Micromechanical Model of Rough Contact between Rock Blocks with Application to Wave Propagation

Anil MISRA and Orestes MARANGOS

Department of Civil Engineering,
University of Kansas, Lawrence, KS, USA
e-mail: amisra@ku.edu

A b s t r a c t

The relationship between effective stiffness of rough contacts of rock blocks and transmission of plane waves is well known. Effective stiffness of a rough contact may be related to the force-deformation behavior of the asperity contacts and the statistical description of rock joint surface topography through micromechanical methods. In this paper, a micromechanical methodology for computing the overall rock contact effective stiffness is utilized along with the imperfectly bonded interface model to investigate how transmitted and reflected wave amplitudes are affected by the incident wave frequency, rock joint closure and the existing rock joint normal stress conditions. As a result, expressions for reflected and transmitted wave amplitudes as well as group time delay of the wave-packets are obtained and parametrically evaluated.

Key words: rough contact, micromechanics, effective stiffness, rock joint, wave propagation.

1. INTRODUCTION

The effective stiffness of the contact between rock blocks has an important role in the geophysical behavior of rock masses and other fractured materials. A number of researchers have investigated the transmission behavior of plane waves through rough surfaces in contact by treating them as imper-

fectly bonded interfaces represented by an effective interface stiffness (see, for example, Kendal and Tabor 1971, Murty 1975, Schoenberg 1980, Murty and Kumar 1991, Pyrak-Nolte *et al.* 1990, Rokhlin and Wang 1991, Gu *et al.* 1996, Pecorari 2003, Nakagawa *et al.* 2004). In these studies, very little attempt has been made to relate the effective interface stiffness to the interface geometry and the mechanical properties of the rock. Contacts between rock blocks are highly inhomogeneous, and because of the surface roughness, occur through local contact areas or asperities. As a result, the transmission of seismic waves through rock joints is influenced by a variety of factors such as the frequency of the incident wave, the rock joint roughness, the mechanical properties of the rock, and the existing normal stress conditions.

The assumption which forms the basis of the wave propagation models based upon the concept of imperfectly bonded interfaces is that the wavelength is much larger than the asperity contact size and asperity contact separation (Pyrak-Nolte and Nolte 1992). Under this assumption, the effective interface stiffness corresponding to interface length scales smaller than the size of wavelength should be considered. Thus, asperity contact stiffnesses at sub-wavelength scales may be averaged to obtain the overall interface stiffness. Asperities, at sub-wavelength scales, consist of different sizes and different orientations giving rise to variation in stiffness between different locations of the rock joint. Micromechanical approaches that explicitly include rock joint surface topography and incorporate material mechanical properties and intrinsic friction may be utilized to obtain the overall interface stiffness.

Recently, the author has developed a kinematically driven micromechanical methodology in which the stress-deformation behavior of a rock joint is obtained by considering the force-deformation behavior of the asperity contacts and the statistical description of rock joint surface topography (Misra 1997, 1999, 2002). The micromechanical methodology developed by the author extends other similar rock-joint models (see, Brown and Scholz 1985, Swan 1983, Yoshioka and Scholz 1989a, b, Boitnott *et al.* 1992, Yoshioka 1997, for a review) by using: (1) a directional distribution function of asperity contact orientations recognizing that the asperity contacts are not equally likely in all directions, and (2) an iterative procedure to obtain the asperity contact forces at each load increment, recognizing that the asperity contact force distribution is not known *a priori*. In the present paper, this micromechanical methodology for computing the overall rock joint stiffness is utilized along with the imperfectly bonded interface model to investigate how transmitted and reflected wave amplitudes are affected by the incident wave frequency, rock joint closure and the existing rock joint normal stress conditions.

In the subsequent discussion, we first briefly describe the essence of the kinematically driven micromechanical methodology. We then employ this model to study the behavior of *P*-wave transmission and reflection under varying rock joint normal stress conditions and initial joint closures and we find that the amplitudes of the reflected and transmitted waves as well as group time delay of the wave-packets are significantly influenced by the joint stress and initial closure conditions. Since the micromechanical method explicitly incorporates the asperity heights and radii of curvature, scale-dependent overall rock joint stiffness may be obtained. The micromechanical model may thus be used to further elucidate the frequency dependency of wave transmission in rock joints.

2. MICROMECHANICAL MODEL OF ROUGH ROCK JOINT

We consider the micromechanical methodology wherein the stress-deformation behavior of a rock joint is obtained by considering the force-deformation behavior of the asperity contacts and the statistical description of rock joint surface topography (Misra 1999). At the asperity contact-level, a local force-deformation relationship is defined that accounts for the elastic deformation and inelastic sliding at the contact. As schematically depicted in Fig. 1, the stress-deformation relationship for a rock joint is then derived by utilizing: (1) the distribution functions of asperity heights and contact orientations, and (2) the overall kinematic constraints and equilibrium conditions for the rock joint.

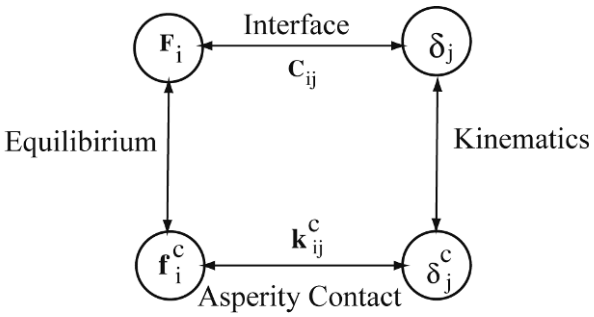

Fig. 1. Schematic depiction of the micromechanical modeling methodology for rock joints.

2.1 Asperity Force-Deformation Relationship

In the kinematically driven approach, the relative motion, δ_j^c, at an asperity contact is decomposed into an elastic part, δ_j^{ce}, and an inelastic sliding part, δ_j^{cp}, given by

$$\delta_j^c = \delta_j^{ce} + \delta_j^{cp} \ . \tag{1}$$

The subscripts in this paper follow the established tensor convention unless specified otherwise. The elastic deformations, δ_j^{ce}, at an asperity contact generate forces, f_i^c, which are related *via* the asperity contact stiffnesses, K_{ij}^c, as follows:

$$f_i^c = K_{ij}^c \, \delta_j^{ce} \, . \tag{2}$$

The asperity contact stiffnesses, K_{ij}^c, generally depend upon the contact loading condition, such as the stiffness given by the Hertzian contact theory (Johnson 1985).

The Amonton–Coulomb's friction law, expressed by the following inequality, governs the sliding at an asperity contact:

$$f_i^c q_i^c \le 0 \, , \tag{3}$$

where $q_i^c = \zeta_i^c + \mu n_i^c$, ζ_i^c is a unit vector in the sliding direction, μ is the asperity friction coefficient and n_i^c is a unit vector outwardly normal to the asperity contact. Combining eqs. (1)-(3), the following relationship between the force and relative motion at a sliding asperity contact may be derived (see, Misra 1997 for more details):

$$f_i^c = K_{ir}^c \left(\delta_{rj} - M^c K_{sj}^c q_s^c \zeta_r^c \right) \delta_j^c \, , \tag{4}$$

where δ_{rj} (= 1 for $r = j$; = 0 for $r \neq j$) is the Kronecker delta and the scalar M^c is given by

$$M^c = \left(K_{ij}^c \zeta_j^c \, q_i^c \right)^{-1} . \tag{5}$$

The asperity force-displacement relationship in eq. (4) is decomposed into an elastic part and an inelastic part as follows:

$$f_i^c = C_{ij}^c \delta_j^c = \left(C_{ij}^{ce} - C_{ij}^{cp} \right) \delta_j^c \, , \tag{6}$$

where C_{ij}^c is the overall asperity contact stiffness tensor composed of an elastic part $C_{ij}^{ce} = K_{ij}^c$ and an inelastic part $C_{ij}^{cp} = K_{ir}^c \, M^c \, K_{sj}^c \, q_s^c \, \zeta_r^c$.

2.2 Statistical Description of Rock Surface

The rock surface geometry determines the orientations and the number of asperity contacts under a given loading condition. The composite topography of contacting rock joint surfaces, described *via* statistics of asperity contact heights, orientations, and curvatures, may be utilized for this purpose (see, Nayak 1971, Adler and Firman 1981, Yoshioka 1994, Misra 1997 among others). In this paper, the statistical distribution of asperity contact heights is

described *via* gamma distributions, and that of asperity contact orientation *via* spherical harmonic expansions.

It is usual to define the asperity contact height with reference to the highest peak of the composite topography such that, asperity height, r, represents the overlap of the interacting surfaces. The density function for asperity heights, $H(r)$, is given by a gamma distribution (see, Adler and Firman 1981, Yoshioka and Scholz 1989) expressed as

$$H(r) = \frac{r^{\alpha}\, \mathrm{e}^{-r/\beta}}{\Gamma(\alpha+1)\,\beta^{\alpha+1}} \qquad (0 < r < \infty,\quad \alpha > -1,\quad \beta > 0), \tag{7}$$

where α and β are the parameters related to the mean and variance of the asperity heights as follows:

$$\begin{aligned} &\text{mean}: && r_m = \beta(\alpha+1), \\ &\text{variance}: && r_\sigma^2 = \beta^2(\alpha+1), \end{aligned} \tag{8}$$

Parameter α is unit less while parameter β takes the unit of asperity height. Figure 2 illustrates the distribution of asperity heights for surfaces with varying roughness. Surfaces that have smaller average asperity height and narrow distributions of asperity heights are considered to be relatively smoother.

For a rock joint with N asperities per unit area, $NH(r)\,\mathrm{d}r$ denotes that number of asperity contacts in the interval represented by r and $r + \mathrm{d}r$. Thus, the total number of asperity contacts, under a given loading condition, is given by

$$N_r = \int_0^r NH(r)\,\mathrm{d}r, \tag{9}$$

where r represents the rock joint closure under a given loading.

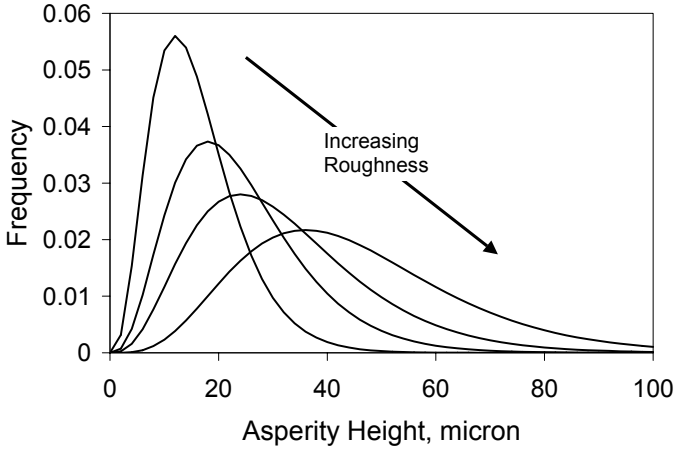

Fig. 2. Asperity height distributions with varying surface roughness.

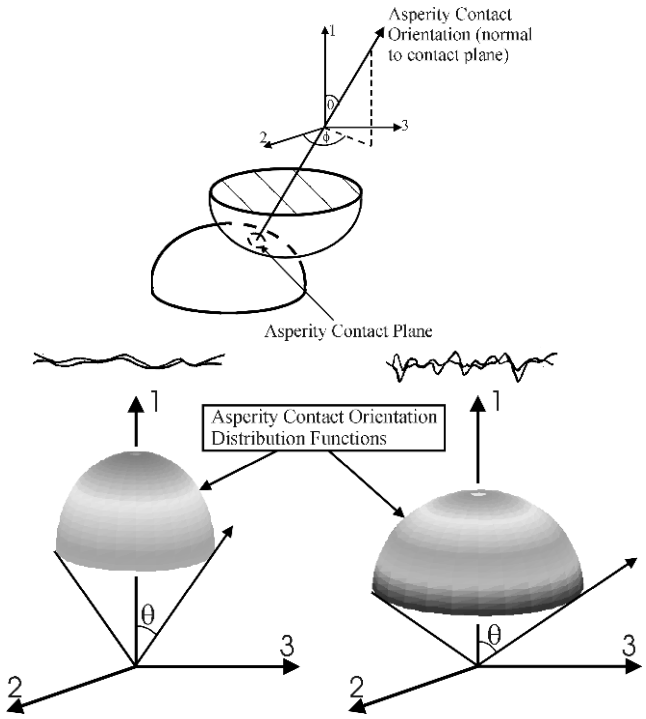

Fig. 3. Schematic depiction of asperity contact orientation distribution functions for smooth and rough interfaces.

The asperity contact orientation is defined by considering the inclination of the asperity contact normal with respect to that of the rock joint surface normal direction. As shown in Fig. 3, the orientation of an oblique asperity contact is defined by the azimuthal angle ϕ and the meridional angle θ, measured with respect to a Cartesian coordinate system in which direction 1 is normal to the rock joint surface.

A 3-dimensional density function utilizing spherical harmonics expansion in spherical polar coordinates that describes the concentrations of asperity contact orientations was introduced by Misra (1997, 1999). For a rock joint with isotropic geometry, the density function, $\xi(\Omega)$, of asperity contact orientations distribution in the domain: $0 \le \theta \le \pi/2a$, $0 \le \phi \le 2\pi$, is given by

$$\xi(\Omega) = \frac{a \sin a\theta}{2\pi \sin\theta}, \qquad (0 \le \theta \le \pi/2a\,; \quad 0 \le \varphi \le 2\pi\,; \quad a \ge 1)\,, \tag{10}$$

where angles ϕ and θ are defined in Fig. 3, Ω represents the solid angle formed by ϕ and θ, and parameter a determines the shape of the density function $\xi(\Omega)$. Thus, the product $N_r \xi(\Omega)\, \mathrm{d}\Omega$ denotes the number of asperity contacts N_Ω in the interval represented by solid angles Ω and $\Omega + \mathrm{d}\Omega$, that is

$$N_\Omega = N_r \xi(\Omega)\, \mathrm{d}\Omega\,. \tag{11}$$

The density function in eq. (10) has the ability to model surfaces with varying roughness. As discussed in Misra (1999), the asperity contacts for smooth surfaces have a greater tendency to concentrate in the direction nor-

mal to the rock joint than that for rough surfaces. It is noteworthy that, as parameter a increases, the contact distribution concentrates towards the direction normal to the interface. In particular, the density function, $\xi(\Omega)$, behaves like a delta function in the limit $a \to \infty$ and yields an expectation $E[\theta] = 0$, which represents a concentrated contact orientation, normal to the interface of a perfectly smooth joint. In general, the parameter a describes the extent of the asperity contacts in the meridional direction as well as the mean asperity contact orientation.

2.3 Effective Stress-Deformation Relationship of Rock Joint

Considering the equilibrium of forces at a rock joint surface, the overall traction F_i on the rock joint is obtained from the summation of the forces, f_i^c, developed at asperities, which for a large number of asperity contacts may be written as the following integral equation:

$$F_i = N \int_r \int_\Omega f_i^c \, \xi(\Omega) \, H(r) \, \mathrm{d}\Omega \, \mathrm{d}r \,, \tag{12}$$

where the traction F_i is given as force per unit area since N is measured per unit area of a rock joint. Under a given loading condition, an asperity contact may be sliding, separated or in elastic contact. Appropriately accounting for the asperity contact forces given by eq. (7), and adopting the kinematic assumption that relative motion at an asperity, δ_j^c, is same as the relative motion of the interface, δ_j, the relationship between the overall traction F_i and the relative motion δ_j may be written as

$$F_i = C_{ij} \, \delta_j = \left[C_{ij}^e - C_{ij}^p \right] \delta_j \,, \tag{13}$$

where the superscripts e and p refer to the elastic and inelastic part of the rock joint stiffness tensor, C_{ij}.

The domain of sliding and separated asperity contacts is not always known *a priori* (Misra 1997, 1999). Moreover, for non-constant asperity contact stiffness and changing surface roughness, the sliding domain evolves with loading. In addition, new asperity contacts are formed and existing contacts lost as the rock joint is sheared. Numerically, the asperity separation may be detected by examining the total relative displacement in the normal direction of an asperity contact. Consequently, an incremental rock joint stress-displacement relationship is obtained by numerically integrating the following equations for each loading step:

$$C_{ij}^e = N \int_0^r \int_0^{2\pi} \int_0^{\pi/2a} K_{ij}^c \;\; \xi(\varphi, \theta) \;\; \sin\theta \; \mathrm{d}\theta \;\; \mathrm{d}\varphi \; H(r) \, \mathrm{d}r \,, \tag{14a}$$

$$C_{ij}^{p} = N\int_{0}^{r}\int_{\varphi_s}\int_{\theta_s} M^{c}\, K_{ik}^{c}\, \zeta_{k}^{c}\, K_{nj}^{c}\, q_{m}^{c}\, \xi(\varphi,\theta)\, \sin\theta\, \mathrm{d}\theta\, \mathrm{d}\varphi\, H(r)\, \mathrm{d}r$$

$$+ N\int_{0}^{r}\int_{\varphi_d}\int_{\theta_d} K_{ij}^{c}\, \xi(\varphi,\theta)\, \sin\theta\, \mathrm{d}\theta\, \mathrm{d}\varphi\, H(r)\, \mathrm{d}r\,, \tag{14b}$$

where $\xi(\phi,\theta)$ is the asperity contact orientation distribution given by eq. (10), $H(r)$ is the asperity height distribution given by eq. (7), $r = r_0 + \delta_1$, r_0 is the initial closure at $\delta_1 = 0$ and the integration is performed over the domain of sliding asperity contacts denoted by superscript s and separated asperity contacts denoted by superscript d.

It is convenient to express the asperity stiffness tensor, K_{ij}^{c}, in terms of asperity stiffness that describes the behavior along the direction of normal and tangent to an asperity contact, such that

$$K_{ij}^{c} = K_{n}^{c} n_{i}^{c} n_{j}^{c} + K_{s}^{c}\left(s_{i}^{c} s_{j}^{c} + t_{i}^{c} t_{j}^{c}\right), \tag{15}$$

where K_n and K_s denote asperity stiffness along the normal and tangential direction of the asperity. The unit vector **n** is normal to the asperity contact surface, and vectors **s** and **t** are arbitrarily chosen on the plane tangential to the asperity contact surface, such that **n s t** forms a local Cartesian coordinate system. It is noted that the stiffness terms that cross-link normal and shear behavior are assumed to be negligible in accordance with the theories for contact of smooth non-conforming bodies. Furthermore, for modeling the rock joint behavior under general loading conditions, non-linear asperity contact stiffness, that depend upon contact forces or displacements are preferable.

Considering the Hertzian contact theory of perfectly smooth elastic surfaces as well as other theories of elasto-plastic interfaces (see, Johnson 1985, Misra 1995), the normal asperity stiffness, K_n, may be taken to depend upon the normal asperity deformation, δ_n, according to the following power law:

$$K_n = \lambda K \delta_n^{\eta}\,, \tag{16}$$

where K, λ and η are constants. The asperity stiffness, K_n, given by eq. (16), becomes identical with the Hertz stiffness for contact of perfectly smooth elastic spheres when

$$\lambda = \frac{2-\nu}{2\,(1-\nu)}, \qquad \eta = \frac{1}{2}, \qquad \text{and} \qquad K = \frac{8G\sqrt{R}}{3(2-\nu)}, \tag{17}$$

where G is the shear modulus, ν is Poisson's ratio and R is asperity radius of curvature. It is noteworthy that the exponent η can vary from 0 for perfectly

plastic to ½ for perfectly elastic behavior at contact of perfectly smooth spherical asperities (Johnson 1985). The tangential asperity stiffness, K_s, has, in general, a complex dependence upon the asperity loading conditions in the tangential direction (Mindlin and Deresiewicz 1953). We use the following truncated series representation for the tangential asperity stiffness K_s (Misra 1999):

$$K_s = \frac{3K_n}{2\lambda}\left[1 - \frac{1}{4\mu\lambda}\frac{\delta_s}{\delta_n} - \frac{1}{24\mu^2\lambda^2}\left(\frac{\delta_s}{\delta_n}\right)^2 - O\left(\frac{\delta_s}{\delta_n}\right)^3\right], \tag{18}$$

which yields a variation from $3K_n/2\lambda$, for vanishingly small asperity shear force, to $1.063K_n/\lambda$, for asperity shear force at incipient sliding condition.

The rock joint behavior under normal stress obtained from the present model is compared in Fig. 4 with the experimental data reported by Brown and Scholz (1985). Solid lines give the calculated curves while the experimental data are indicated by symbols. The calculated curves were obtained using the following stiffness parameters: $\eta = 0.5$, $K = 108$ GPa·μm$^{1/2}$, and $\lambda = 1.14$. These stiffness parameters are calculated using the Hertzian stiffness parameters given in eq. (17) for a shear modulus $G = 23$ GPa, Poisson's ratio $\nu = 0.224$, and asperity radius of curvature $R = 9.9$ μm. The asperity contact orientation parameter is taken as $a = 4.4$ for the mean slope of 12.9°, and the asperity height distributions parameters are taken to be $\alpha = 10.39$, $\beta = 3.32$ for the mean and standard deviation of asperity height = 37.8 μm and 11.2 μm, respectively. These parameters are based upon the material and surface geometry information provided in Brown and Scholz (1985). The contact density is taken to be $N = 66.7$ per mm^2, and the asperity friction coefficient 0.3. The behavior critically depends upon the initial closure. To determine the initial closure a parametric study was performed and the initial closure, r_0, was found to be 11 μm.

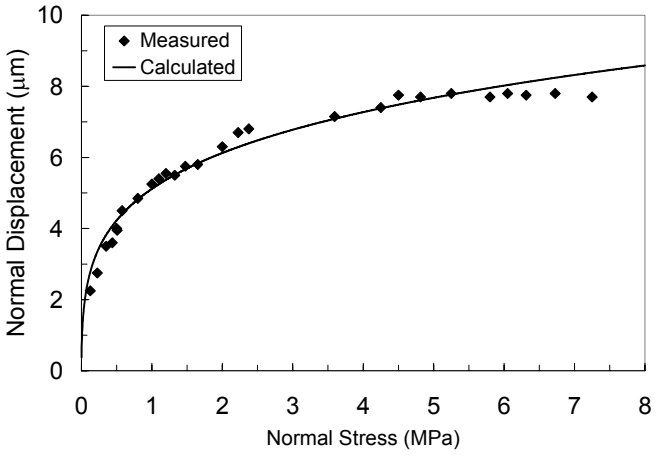

Fig. 4. Measured and calculated rock joint behavior under normal stress.

As seen from Fig. 4, rock joint closure behavior under normal stresses is highly non-linear. The rock joint normal stiffness, C_{11}, given by the slope of the stress-displacement curve also increases nonlinearly with the normal stress. There are two sources of this non-linearity; one due to the formation of new asperity contacts as the rock joint is loaded, and the other due to the non-linear nature of the asperity contact stiffness under oblique loading as given by eqs. (16) and (18). The micromechanical model accurately describes the non-linearity of the closure behavior.

3. REVIEW OF WAVE PROPAGATION MODELING THROUGH ROUGH CONTACTS

The micromechanical model described above is applied to investigate wave propagation through rock joints based upon the imperfectly bonded interface methodology, also known as linear slip or displacement discontinuity approach (Schoenberg 1980, Pyrak-Nolte *et al.* 1990, Gu *et al*. 1996, Pecorari 2003). In the subsequent description we focus upon incident *P* waves only; however, we note that incident *SV* and *SH* waves may be treated in a similar manner. We also give a brief description of the imperfectly bonded interface methodology in order to define the appropriate quantities.

In general, an incident *P* wave on an interface will produce reflected and transmitted *P* and *SV* waves. The displacements due to the incident, reflected and transmitted waves may be represented as (Achenbach 1973)

$$u_i^{(n)} = A_n d_i^{(n)} \exp\left(\mathrm{i}\frac{\omega}{c_n}(x_i p_i^{(n)} - c_n t) \right), \tag{19}$$

where d_i is the unit vector defining the direction of motion, p_i is the unit vector defining the direction of propagation, x_i is the position vector, c_n is the phase velocity, A_n is the amplitude of the n-th phase, and ω is the cyclic frequency of the wave. Subscript n designate the different phases. For the incident wave, $n = 0$. The reflected *P* and *SV* waves are assigned the values $n = 1$ and $n = 2$, respectively, while the transmitted *P* and *S* waves are assigned the values $n = 3$ and $n = 4$, respectively. Other subscripts follow the usual tensor notation. Now, using eq. (19), the n-th phase stress tensor in an elastic body may be written as

$$\tau_{lm}^{(n)} = \left[\lambda \delta_{lm} (d_j^{(n)} p_j^{(n)}) + \mu \left(d_l^{(n)} p_m^{(n)} + d_m^{(n)} p_l^{(n)} \right) \right] \mathrm{i}\frac{\omega}{c_n} A_n \exp\left(\mathrm{i}\frac{\omega}{c_n}(x_i p_i^{(n)} - c_n t) \right), \tag{20}$$

where λ and μ are the material Lame's constants.

For convenience, we choose a coordinate system, such that the direction of incident *P*-wave propagation is within the 1-2 plane shown in Fig. 3.

At an imperfect interface, the tractions in the upper medium, A, are equal to the tractions in the lower medium, B, as follows (see, Schoenberg 1980 among others):

$$F_1^A = F_1^B = F_1 \quad \text{and} \quad F_2^A = F_2^B = F_2 \,. \tag{21}$$

The displacements at an imperfect interface are considered to be discontinuous such that the force boundary conditions are given by

$$F_1 = C_{11}\delta_1 = C_{11}(u_1^B - u_1^A)\,, \tag{22a}$$

$$F_2 = C_{22}\delta_2 = C_{22}(u_2^B - u_2^A)\,, \tag{22b}$$

where $F_1 = \tau_{11}$, $F_2 = \tau_{12}$, and C_{11} and C_{22} are the rock joint normal and shear stiffnesses, respectively, given by eq. (13).

For same upper and lower media, eqs. (19) through (22) may be combined to obtain the amplitudes of the reflected and transmitted P and SV waves for an asperity in contact as follows:

$$[\mathrm{T}] \begin{Bmatrix} R_P \\ R_{SV} \\ T_P \\ T_{SV} \end{Bmatrix} = \begin{Bmatrix} -\cos\theta \\ \sin\theta \\ \cos 2\theta_2 \\ \sin 2\theta \end{Bmatrix}, \tag{23}$$

where the matrix [T] is given as

$$\begin{bmatrix} -\cos\theta & \sin\theta_2 & -\cos\theta + \mathrm{i}\left(\dfrac{\omega}{C_{11}}\right)c_P\rho\cos 2\theta_2 & -\sin\theta_2 + \mathrm{i}\left(\dfrac{\omega}{C_{11}}\right)c_{SV}\rho\sin 2\theta_2 \\ -\sin\theta & -\cos\theta_2 & \sin\theta - \mathrm{i}\left(\dfrac{\omega}{C_{22}}\right)\dfrac{{c_{SV}}^2}{c_P}\rho\sin 2\theta & -\cos\theta_2 + \mathrm{i}\left(\dfrac{\omega}{C_{22}}\right)c_{SV}\rho\cos 2\theta_2 \\ -\cos 2\theta_2 & \dfrac{c_{SV}}{c_P}\sin 2\theta_2 & \cos 2\theta_2 & \dfrac{c_{SV}}{c_P}\sin 2\theta_2 \\ \sin 2\theta & \dfrac{c_P}{c_{SV}}\cos 2\theta_2 & \sin 2\theta & \dfrac{c_P}{c_{SV}}\cos 2\theta_2 \end{bmatrix} \tag{24}$$

where $R_P = A_1/A_0$ and $R_{SV} = A_2/A_0$ are the P- and SV-wave reflection coefficients, $T_P = A_3/A_0$ and $T_{SV} = A_4/A_0$ are the P- and SV-wave transmission coefficients, θ is the wave incidence angle, θ_2 is obtained from Snell's law, c_P and c_{SV} are the P- and SV-wave velocities in the rock, and ρ is the rock mass density. At normal incidence ($\theta = 0$) an incident P wave on the rock joint will produce only a reflected and a transmitted P wave, for which the closed form solutions of normalized reflected and transmitted wave amplitudes and phase angles, respectively, are obtained as (general expressions of

normalized reflected and transmitted wave amplitudes for oblique incidence are given in Gu *et al*. 1996).

$$\left|R_P\right| = \frac{1}{\sqrt{\dfrac{4C_{11}^2}{c_P^2\rho^2\omega^2}+1}}, \qquad \left|T_P\right| = \frac{1}{\sqrt{1+\dfrac{\omega^2 c_P^2\rho^2}{4C_{11}^2}}}, \tag{25}$$

$$\varphi_R = -\tan^{-1}\left(\frac{2C_{11}}{\omega c_P\rho}\right), \quad \varphi_T = \tan^{-1}\left(\frac{\omega c_P\rho}{2C_{11}}\right). \tag{26}$$

Interestingly, the phase angles are a function of the frequency. Thus, for a wave packet transmitting through the rock joint, the group time delay may be obtained as the rate of change of phase angle with respect to frequency as follows:

$$t_g = \frac{2c_P\rho C_{11}}{4C_{11}^2+\left(\omega c_P\rho\right)^2}. \tag{27}$$

4. PARAMETRIC RESULTS FOR REFLECTION AND TRANSMISSION AT ROCK JOINT

In order to evaluate the transmission and reflection coefficients and group time delay for a rock joint using eqs. (25) and (27), a numerical effort is required as the rock joint stiffness is non-linearly dependent upon the joint closure. Moreover, the joint closure, *r*, is a function of the rock joint normal stress. In the parametric study described below, we consider an incident *P* wave that is propagating in a direction normal to the rock joint. We calculate the reflected and the transmitted *P*-wave amplitudes and group time delay as a function of the incident wave frequency and existing normal stress conditions for the rock joint whose closure behavior is given in Fig. 4. The *P*-wave velocity for this rock is computed to be 4638 m/s and the density is taken to be 3 Mg/m^3. The normal stiffness C_{11} is computed using the parameters given in Section 2.3. We also study the effect of rock joint initial closure on the wave transmission behavior.

4.1 Effect of incident wave frequency and normal stress

In Figure 5, we show the normalized amplitudes of the reflected and transmitted *P* waves as a function of frequency for three different normal stress conditions. Classical reflection and transmission coefficient versus frequency curves are obtained. As expected the reflected *P*-wave amplitude increases to an asymptotic value of 1 while the transmitted *P*-wave amplitude decreases to an asymptotic value of 0. However, the rate at which the curves reach the asymptote significantly depends upon the rock joint normal stress.

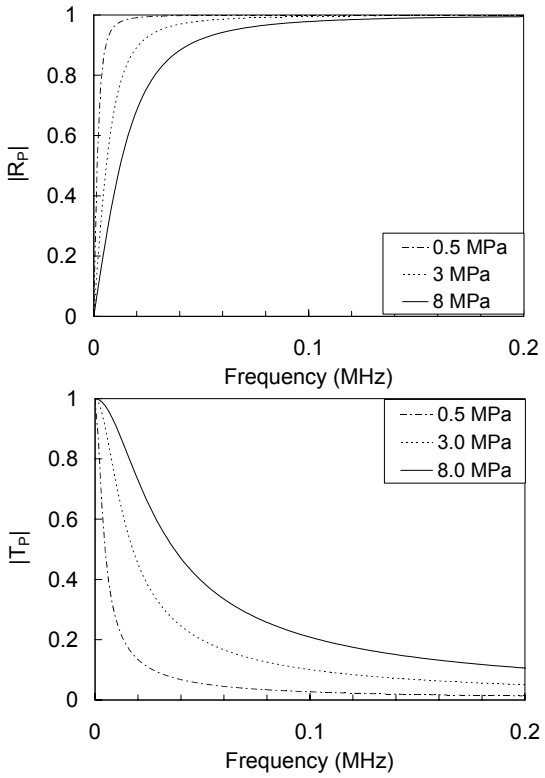

Fig. 5. Effect of wave frequency and normal stress upon reflected and transmitted wave amplitudes.

At a given normal stress on the rock joint, only low frequency incident *P* waves transmit through, while the high frequency waves are mostly reflected back. Thus the rock joint acts as a low-pass filter, as observed by Pyrak-Nolte and Nolte (1992). It is noteworthy that both the reflected and transmitted *P*-wave amplitude has a nonlinear dependence upon the rock joint normal stress condition, which reflects the non-linear variation of rock joint normal stiffness C_{11} with normal stress. For a given frequency, say at 10 kHz, the transmitted *P*-wave amplitude initially increases rapidly at low stress-levels, and subsequently increases slowly at higher stress-levels. The nonlinear behavior is attributable to the formation of new contacts as the normal stress is increased. Furthermore, a majority of the new contact formation occurs at relatively low normal stresses. Therefore, the nonlinearity of the initial normal stiffness with normal stress diminishes at higher normal stresses. Most of the gain in stiffness at higher stress is attributable to deformation hardening caused by non-linear asperity contact behavior. At frequencies above 100 kHz, the transmitted *P*-wave amplitude is typically less than 10% of the incident wave, while the reflected *P*-wave amplitude is typically higher than 90% of the incident wave for the rock joint considered in this paper. At higher frequencies, when wavelength and the asperity contact sizes become comparable, the applicability of the present method is questionable.

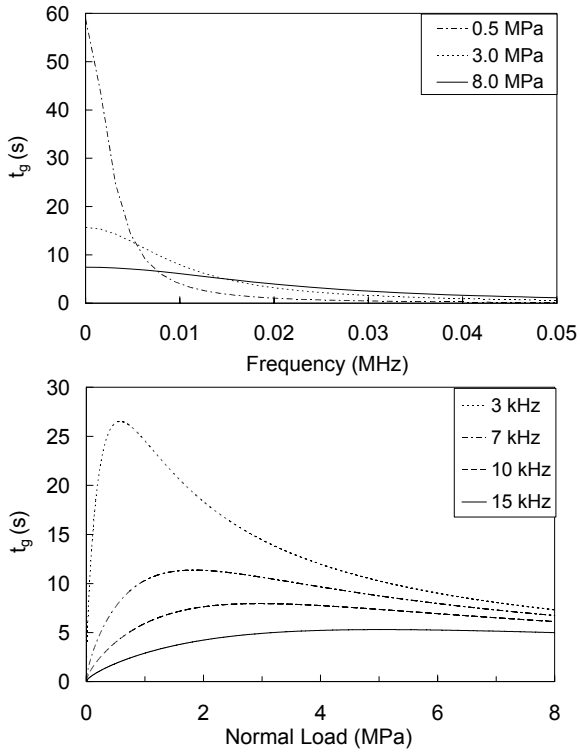

Fig. 6. Effect of wave frequency and normal stress upon group time delay of the transmitted wave packet.

In Fig. 6, we show the group time delay of transmitted *P*-wave packets as a function of central frequency for three different normal stress conditions. We also show the group time delay of transmitted *P*-wave packets as a function of normal stress for four different central frequencies. The group time delay generally decreases as the frequency increases. However, we observe that the group time delay behavior at different frequencies depends upon the rock joint normal stress. For very low frequencies, the group time delay is less at higher values of normal stress. For higher frequencies, the time group delay is less at lower values of normal stress.

For a given frequency, the time group delay displays a maximum at specific value of normal stress. The magnitude of the maximum and the normal stress at which the maximum occurs depends upon the frequency. For low frequencies, the maximum value is higher and occurs at lower normal stresses. As the frequency increases, the magnitude of the maximum value decreases and the normal stress at which the maximum occurs shifts to higher values. Furthermore, at high normal stress, the group time delay is independent of frequency and seems to converge to a constant.

4.2 Effect of rock joint initial closure

The rock joint initial closure, which may result from joint mismatch, has a significant influence on the reflected and transmitted wave amplitudes for

given joint normal stress condition and wave frequency. Since the number of asperity contacts increases non-linearly with initial closure, the joint normal stiffness, C_{11}, and therefore the reflected and transmitted wave amplitudes also vary nonlinearly with initial closure. In Figs. 7 and 8 we show the normalized amplitudes of the reflected and transmitted *P* waves as a function of initial joint closure for: (1) two frequencies at the normal stress of 0.5 MPa, and (2) two normal stresses at the wave frequency of 0.01 MHz, respectively.

As seen from Fig. 7, the rate of normalized amplitude variation with initial closure critically depends upon the wave frequency at a constant joint normal stress. For instance, the rate at which the reflected wave amplitude decreases becomes considerably slower at high frequencies. At a given normal stress, the joint stiffness is related to the contact stiffness, which, in turn, is proportional to the asperity contact size represented by the asperity radius of curvature. *P* waves with wavelengths comparable to the asperity contact size are likely to be scattered or reflected. Therefore, at frequencies higher than certain critical frequency, the reflection coefficients are high and change minimally with the number of contacts. The micromechanical model used to calculate the normal stiffness reasonably predicts this phenomenon.

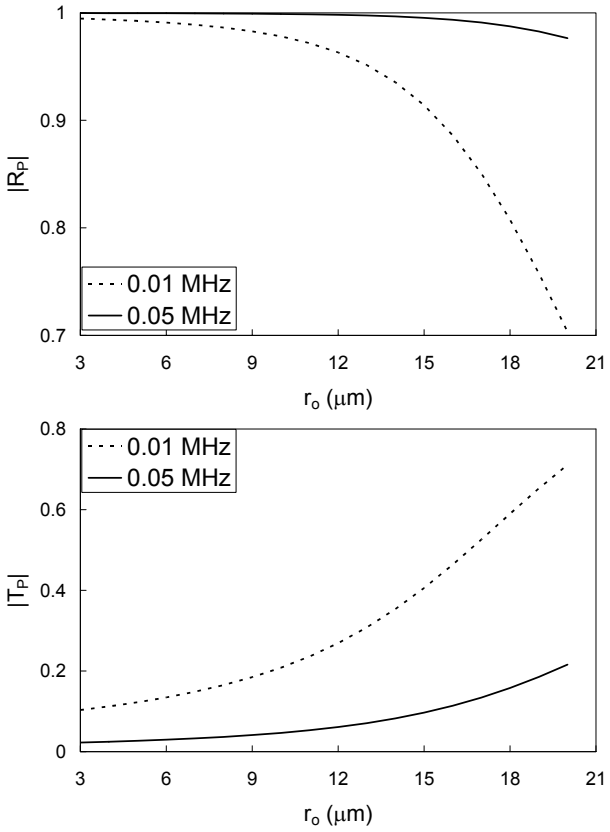

Fig. 7. Effect of initial closure upon reflected and transmitted wave amplitudes for a joint normal stress of 0.5 MPa.

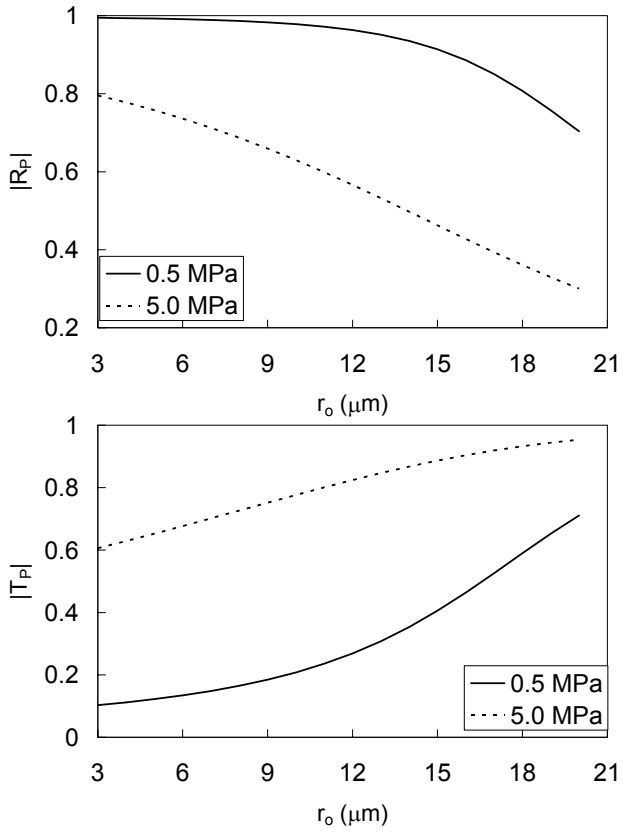

Fig. 8. Effect of initial closure upon reflected and transmitted wave amplitudes for wave frequency of 0.01 MHz.

For a given frequency, on the other hand, the reflected and transmitted wave amplitudes variation with initial closure depends significantly upon the joint normal stress, as shown in Fig. 8. At low initial closure, the number of asperity contacts is smaller. Thus, for a higher rock joint normal stress, the same number of asperity contacts has to carry a higher contact force per asperity. Since the asperity stiffness has a non-linear dependence on contact force, higher contact force results in considerably higher asperity stiffness. As the initial closure becomes larger, the number of asperity contacts increases, which has the propensity to increase the overall joint stiffness. However, for higher number of asperities, the asperity contact forces will tend to be relatively lower, and hence, the asperity stiffness is smaller. Thus, the increase in overall joint stiffness with initial closure at a given normal stress combines the two competing effects. The variation in the reflected and transmitted wave amplitudes with initial closure reflects the result of these competing effects on the overall joint stiffness. Moreover, as the overall joint stiffness becomes higher, the reflected and transmitted wave amplitudes approach their asymptotic values of 0 and 1, respectively, resulting in a sigmoidal-like behavior with initial closure.

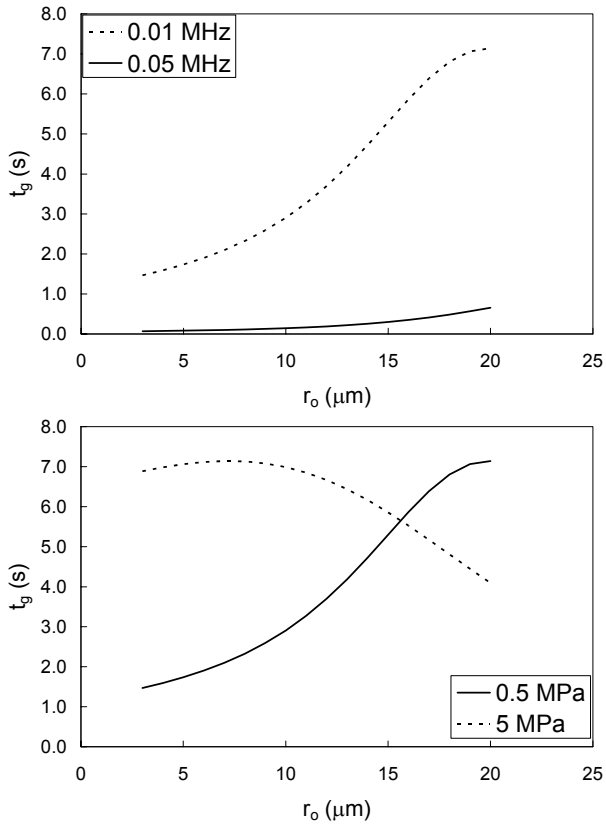

Fig. 9. Effect of wave frequency and normal stress upon group time delay of the transmitted wave packet.

In Fig. 9, we show the group time delay of transmitted *P*-wave packets as a function of initial closure for: (1) two frequencies at the normal stress of 0.5 MPa, and (2) two normal stresses at the central frequency of 0.01 MHz. In general, the group time delay increases with joint stiffness, and consequently, with the joint initial closure to a maximum value at a critical initial closure. Beyond the critical initial closure, the group time delay decreases. The group time delay and the critical initial closure depend upon the frequency and the joint normal stress. For a given normal stress, the group time delay is lower and the critical initial closure higher at the higher frequencies. On the other hand, for a given frequency, higher group time delays are achieved at lower initial closure for higher joint normal stress. Thus, the maximum group time delay occurs at a lower critical initial closure at higher joint normal stress.

5. CONCLUDING REMARKS

A kinematically driven micromechanical methodology for computing the overall rock joint stiffness is utilized along with the imperfectly bonded interface model to investigate how the transmitted and reflected wave ampli-

tudes are affected by the incident wave frequency, rock joint closure and the existing rock joint normal stress conditions. In the micromechanical methodology, an effective stress-deformation behavior of a rock joint is obtained by considering the force-deformation behavior of the asperity contacts and the statistical description of rock joint surface topography. This micromechanical methodology incorporates: (1) a directional distribution function of asperity contact orientations recognizing that the asperity contacts are not equally likely in all directions, and (2) an iterative procedure to obtain the asperity contact forces at each load increment, recognizing that the asperity contact force distribution is not known *a priori*. The rock joint stiffness predicted by the micromechanical method is used to obtain the reflected and transmitted wave amplitudes as well as wave-packet group time delay for various frequency, joint normal stress and initial closure.

The advantage of using a micromechanical model in this analysis is that it gives a physical explanation as to how the wave propagation through rock joints is affected by the interface geometry and mechanical properties of the rock. Since the micromechanical method explicitly incorporates the asperity heights and radii of curvature, it is possible to obtain scale-dependent overall rock joint stiffness. The micromechanical model may thus be used to further elucidate the frequency dependency of wave transmission in rock joints. Consequently, this type of model could potentially be used to solve the inverse problem of determining existing normal stress conditions, interface geometry and mechanical rock joint properties from acoustic wave propagation.

Based upon the parametric study, we find that the frequency dependent amplitudes of the reflected and transmitted waves as well as group time delay of the wave-packets are significantly influenced by the joint stress and initial closure conditions. The reflected and transmitted wave amplitudes and the group time delay of the wave-packets have a highly nonlinear dependence upon the rock joint normal stress condition and initial closure. This nonlinearity is directly related to the nonlinear relationship between the joint normal stiffness and normal stress condition predicted by the micromechanical model.

References

Achenbach, J.D. (1973), *Wave Propagation in Elastic Solids*, North Holland, New York.

Adler, R.J., and D. Firman (1981), A non-Gaussian model for random surfaces, *Phil. Trans. Roy. Soc. Lond. A* **303**, 433-462.

Boitnott, G.N., R.L. Biegel, C.H. Scholz, N. Yoshioka, and W. Wang (1992), Micromechanics of rock friction 2. Quantitative modeling of initial friction with contact theory, *J. Geophys. Res*. **97**, 8965-8978, DOI: 10.1029/92JB00019.

Brown, S.R., and C.H. Scholz (1985), Closure of random elastic surfaces in contact, *J. Geophys. Res.* **90**, B7, 5531-5545, DOI: 10.1029/JB090iB07p05531

Brown, S.R., and C.H. Scholz (1986), Closure of rock joints, *J. Geophys. Res*. **91**, B7, 4939-4945, DOI: 10.1029/JB091iB05p04939.

Gu, B., R. Suarez-Rivera, K.T. Nihei, and L.R. Myer (1996), Incidence of plane waves upon a fracture, *J. Geophys. Res.* **101**, B11, 25337-25346.

Johnson, K.L. (1985), *Contact Mechanics*, Cambridge University Press, London.

Kendal, K., and D. Tabor (1971), An ultrasonic study of area of contact between stationary and sliding surfaces, *Proc. R. Soc. A* **323**, 321-340, DOI: 10.1098/rspa.1971.0108.

Mindlin, R.D., and H. Deresiewicz (1953), Elastic spheres in contact under varying oblique forces, *J. Appl. Mech*. **20,** 3, 327-344.

Misra, A. (1995), Interfaces in particulate materials. **In:** A.P.S. Selavadurai and M.P. Boulon (eds.), *Mechanics of Geomaterial Interfaces*, 513-536, Elsevier Sci., New York, DOI: 10.1016/S0922-5382(06)80024-3.

Misra, A. (1997), Mechanistic model for contact between rough surfaces, *J. Eng. Mech.*, **123**, 5, 475-484, DOI: 10.1061/(ASCE)0733-9399(1997)123:5(475).

Misra, A. (1999), Micromechanical model for anisotropic rock joints, *J. Geophys. Res*. **104,** 23175-23187, DOI: 10.1029/1999JB900210.

Misra, A. (2002), Effect of asperity damage on shear behavior of single fracture, *Eng. Fracture Mech*. **69**, 17, 1997-2014, DOI: 10.1016/S0013-7944(02)00073-5.

Murty, G.S. (1975), A theoretical for the attenuation and dispersion of stoneley waves at the loosely bonded interface of elastic half-space, *Phys. Earth. Planet. Int.* **11**, 65-79, DOI: 10.1016/0031-9201(75)90076-X.

Murty, G.S., and V. Kumar (1991), Elastic wave propagation with kinematics discontinuity along a non-ideal interface between two isotropic elastic half-spaces, *J. Nondest. Eval.* **10**, 2, 39-53, DOI: 10.1007/BF00568099.

Nagy, P.B. (1992), Ultrasonic classification of imperfect interfaces, *J. Nondest. Eval*. **11**, 3/4, 127-139, DOI: 10.1007/BF00566404.

Nakagawa, S., K.T. Nihei, and L.R. Myer (2004), Plane wave solution for elastic wave scattering by heterogeneous fracture, *J. Acoust. Soc. Am*. **115**, 6, 2761-2772, DOI: 10.1121/1.1739483.

Nayak, P.R. (1971), Random process model of rough surfaces, *J. Lubr. Technol*. **93**, 398-407.

Pecorari, C. (2003), Nonlinear interaction of plane ultrasonic waves with an interface between rough surfaces in contact, *J. Acoust. Soc. Am*. **113**, 6, 3065-3072, DOI: 10.1121/1.1570437.

Pyrak-Nolte, L.J., and D.D. Nolte (1992), Frequency dependence of fracture stiffness, *Geophys. Res. Lett*. **19**, 3, 325-328, DOI: 10.1029/91GL03179.

Pyrak-Nolte, L.J, L.R. Myer, and N.G.W. Cook (1990), Transmission of seismic waves across single natural fractures, *J. Geophys. Res*. **95**, 8617-8638, DOI: 10.1029/JB095iB06p08617.

Rokhlin, S.I., and Y.J. Wang (1991), Analysis of boundary conditions for elastic wave interaction with an interface between two solids, *J. Acoust. Soc Am*. **89**, 503-515, DOI: 10.1121/1.400374.

Schoenberg, M. (1980), Elastic wave behavior across linear slip interfaces, *J. Acoust. Soc Am*. **68**, 1516-1521, DOI: 10.1121/1.385077.

Swan, G. (1983), Determination of stiffness and other joint properties from roughness measurements, *Rock Mech. Rock Eng*. **16**, 19-38, DOI: 10.1007/BF01030216.

Yoshioka, N. (1994), Elastic behavior of contacting surfaces under normal loads: A computer simulation using three-dimensional surface topographies, *J. Geophys. Res*. **99**, 15549-15560, DOI: 10.1029/94JB00938.

Yoshioka, N. (1997), A review of the micromechanical approach to the physics of contacting surfaces, *Tectonophysics* **277**, 29-40, DOI: 10.1016/S0040-1951(97)00076-0.

Yoshioka, N., and C.H. Scholz (1989a), Elastic properties of contacting surfaces under normal and shear loads. 1: Theory, *J. Geophys. Res*. **94**, 17681-17690, DOI: 10.1029/JB094iB12p17681.

Yoshioka, N., and C.H. Scholz (1989b), Elastic properties of contacting surfaces under normal and shear loads. 2: Comparison of theory with experiment, *J. Geophys. Res.* **94**, 17691-17700, DOI: 10.1029/JB094iB12p17691.

Received 1 April 2008
Accepted 16 June 2008